Zoology 117 (2014) 48–56

Contents lists available at ScienceDirect

Zoology

journal homepage: www.elsevier.com/locate/zool

The role of mechanical resonance in the neural control of swimming in fishes☆

Eric D. Tytell[a,*], Chia-Yu Hsu[b], Lisa J. Fauci[c]

[a] Department of Biology, Tufts University, 200 Boston Avenue, Suite 4700, Medford, MA 02155, USA
[b] Department of Applied Mathematics, Feng Chia University, Taiwan
[c] Department of Mathematics, Tulane University, 6823 Saint Charles Avenue, New Orleans, LA 70118, USA

ARTICLE INFO

Article history:
Received 11 September 2013
Received in revised form 25 October 2013
Accepted 30 October 2013
Available online 21 December 2013

Keywords:
Resonance
Entrainment
Stiffness
Damping
Central pattern generator

ABSTRACT

The bodies of many fishes are flexible, elastic structures; if you bend them, they spring back. Therefore, they should have a resonant frequency: a bending frequency at which the output amplitude is maximized for a particular input. Previous groups have hypothesized that swimming at this resonant frequency could maximize efficiency, and that a neural circuit called the central pattern generator might be able to entrain to a mechanical resonance. However, fishes swim in water, which may potentially damp out many resonant effects. Additionally, their bodies are elongated, which means that bending can occur in complicated ways along the length of the body. We review previous studies of the mechanical properties of fish bodies, and then present new data that demonstrate complex bending properties of elongated fish bodies. Resonant peaks in amplitude exist, but there may be many of them depending on the body wavelength. Additionally, they may not correspond to the maximum swimming speed. Next, we describe experiments using a closed-loop preparation of the lamprey, in which a preparation of the spinal cord is linked to a real-time simulation of the muscle and body properties, allowing us to examine resonance entrainment as we vary the simulated resonant frequency. We find that resonance entrainment does occur, but is rare. Gain had a significant, though weak, effect, and a nonlinear muscle model produced resonance entrainment more often than a linear filter. We speculate that resonance may not be a critical effect for efficient swimming in elongate, anguilliform swimmers, though it may be more important for stiffer carangiform and thunniform fishes.

1. Introduction

Nearly all objects that bend or flex have a natural frequency: a frequency at which they naturally tend to oscillate. At the natural frequency, a minimal force input produces a maximum motion output. For example, a clock pendulum relies on the natural frequency of the clock's spring to keep swinging back and forth. Arms and legs are also like pendulums, and humans will spontaneously swing their arms at the natural frequency of their shoulder joints (Hatsopoulos and Warren, 1996), potentially reducing the energy required for locomotion (Ahlborn et al., 2006; Goodman et al., 2000; Verdaasdonk et al., 2006). Can fishes, whose body and appendages are not like pendulums, benefit from similar energy savings?

The natural frequency is a simple consequence of a mechanical system that has a restoring and damping force (Hartog, 1985; Hatsopoulos and Warren, 1996). For example, for a pendulum or a swinging arm or leg, the restoring force is gravity: the higher the angle of the pendulum away from vertical, the stronger the component of the gravitational force that pushes it back toward vertical. Springs also tend to exhibit resonance: the more they are compressed, the stronger they push back. If a spring is compressed by an object with mass m, the restoring force F_{rest} is proportional to the displacement x: $F_{rest} = kx$, where k is a spring constant. The damping force, in turn, is proportional to the velocity $\dot{x}$: $F_{damp} = b\dot{x}$, where a dot represents a time derivative and b is a damping constant. Thus, the total force balance on the object is

$$m\ddot{x} + b\dot{x} + kx = f_{in}, \tag{1}$$

where $\ddot{x}$ is the acceleration and F_{in} is an input force. Dividing by the mass m, this equation is normally written

$$\ddot{x} + 2\zeta\omega_r\dot{x} + \omega_r^2 x = \frac{F_{in}}{m}, \tag{2}$$

where $\omega_r = \sqrt{k/m}$ is the undamped natural frequency and $\zeta = b/(2\sqrt{mk})$ is the damping ratio. When ζ is less than 1, the system is called underdamped, and if the input force is periodic with a frequency near ω_r, the output oscillations in x can be very large (a resonant peak): much larger than if the input has a frequency below

☆ This article is part of a special issue entitled "Axial systems and their actuation: new twists on the ancient body of craniates".

* Corresponding author. Tel.: +1 617 627 0312.
E-mail address: eric.tytell@tufts.edu (E.D. Tytell).

0944-2006/$ – see front matter © 2014 Elsevier GmbH. All rights reserved.
http://dx.doi.org/10.1016/j.zool.2013.10.011

or above ω_r. The location of the resonant peak shifts lower as damping increases. If ζ is greater than 1, the system is overdamped, and does not have a resonant peak. Regardless of the damping, close to the resonant frequency the motion will be 90° out of phase with the input force, another indication of resonance.

Therefore, swinging a pendulum-like arm or leg should require minimal energy input at the resonant frequency, provided the damping is low. Previous studies have shown that animals do tend to walk or run near the resonant frequency of their limbs (Hatsopoulos and Warren, 1996; Williamson, 1998) and that this may contribute to energy savings (Pelc et al., 2008; Verdaasdonk et al., 2006). Moreover, a swinging limb near its resonant frequency is more predictable and simpler to stabilize (Goodman et al., 2000).

For efficient locomotion, it would make sense that the nervous systems of animals could have evolved to take advantage of resonance. The properties of a neural circuit for locomotion, called a central pattern generator (CPG), may allow it to detect a resonant peak and match the resonant frequency. CPG circuits are found in both vertebrates and invertebrates and produce the basic muscle activation patterns for locomotion (Orlovsky et al., 1999; Grillner, 2003; Mullins et al., 2011); they also respond to sensory inputs during the locomotory cycle (Rossignol et al., 2006). A number of studies have indicated that simple CPGs, when connected in a feedback loop with a mechanical system, can converge on the mechanical resonant frequency, a phenomenon called "resonance entrainment" (Hatsopoulos, 1996; Iwasaki and Zheng, 2006; Williams and DeWeerth, 2007), potentially resulting in more efficient and stable locomotion.

Can aquatic organisms benefit from the same savings? Fishes and other organisms do not have pendulum-like limbs, and the water introduces fluid dynamic forces, but their bodies and fins are elastic, and so they might benefit from resonance.

The present study is divided into two parts. In the first, we address the question of whether fish bodies might have a mechanical resonance and what form that resonance might take, presenting data from a computational model of lamprey (*Ichthyomyzon unicuspis*) swimming. In the second part, we consider resonance entrainment, summarizing results from several computational and experimental studies, and then present data from a closed-loop preparation of the lamprey CPG.

2. Is there resonance underwater?

Fish bodies are elastic (Aleyev, 1977; Long et al., 2002a), but internal damping (Long et al., 2002b) and the fluid around them may contribute substantial damping forces. Somewhat surprisingly, given the complex internal anatomy of fishes, almost all previous results have indicated that they bend like a homogeneous elastic beam (Katz et al., 1999; Long et al., 2002a). Thus, as a first approximation we can treat a section of a fish's body as a damped harmonic oscillator (like Eq. (2)), with a nonlinear term introduced by the fluid:

$$\ddot{x} + \underbrace{2\zeta\omega_r\dot{x}}_{internal} + \underbrace{C\dot{x}^2}_{drag} + \omega_r^2 x = \frac{F_{in}}{m}, \tag{3}$$

where C is a parameter that represents the scaling of the side-to-side drag force on a segment of the body:

$$C = \frac{1}{2}\frac{\rho S C_D}{m}, \tag{4}$$

and ρ is the fluid density, S is an area (in this case, usually the lateral projected area or the wetted surface area), and C_D is a drag coefficient. This model represents bending at a single "joint" along the fish's body, and so it neglects many important features of an elongated swimmer, but it is used to illustrate the importance of fluid damping. A more sophisticated model (Ramananarivo et al., 2011) found similar effects when they included a nonlinear drag force.

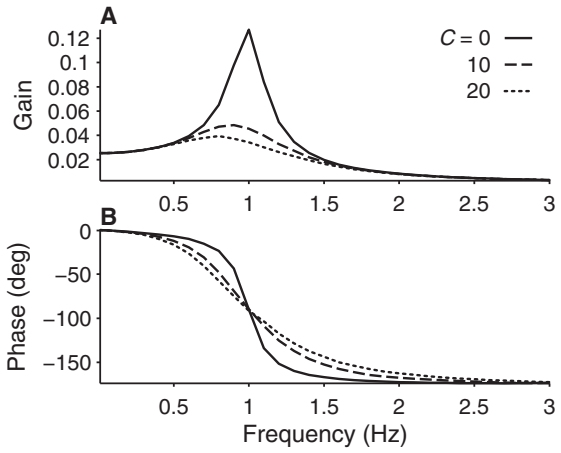

Fig. 1. Hydrodynamic damping can eliminate a resonant peak. Plots show the gain and phase for an underdamped harmonic oscillator ($\zeta = 0.1$) with fluid forces. (A) Gain of the output position with respect to the input force for three different values of the hydrodynamic damping coefficient C (solid line: $C = 0$; dashed: $C = 10$; dotted: $C = 0.1$). (B) Phase of the output position relative to the input force.

If the damping is large, either internally or due to drag, a system like that in Eq. (3) will not have a resonant peak. For a fish that has about the same density as water, $m = \rho V$, where V is a volume, and C_D is between 1 and 2 (for side-to-side oscillations) (Hoerner, 1965). The "fluid dynamic damping" is therefore of the order S/V, and it will only be large if the volume is relatively small compared to the area, which is not true for a cylinder or sphere, but is true for a flat plate – or a fish's tail fin – moving from side to side. Thus, even if fish bodies are elastic and not heavily damped internally, fluid drag may damp out any resonant peak.

Fig. 1 shows an example simulation of such a system (Eq. (3)) with $\zeta = 0.1$ and $f_r = \omega_r/2\pi = 1$ Hz, for a range of fluid dynamic damping values. For a sinusoidal forcing, the nonlinear damping term means that the output is not necessarily sinusoidal, but we can still estimate the gain (the ratio of the output amplitude to the input amplitude) and the phase offset between the output and input (Fig. 1). Even the medium fluid damping (dashed line) nearly eliminates the resonant peak. Ramananarivo et al. (2011) found a similar lack of resonance for flapping wings as long as they included the nonlinear effects of drag.

3. Do fish bodies have a useful mechanical resonance?

Consistent with the idea that fish bodies may be overdamped due to fluid effects, McHenry et al. (1995) found no clear resonant effects in a silicone model of a pumpkinseed sunfish (*Lepomis gibbosus*). They cast elastomer models with the same shape as a sunfish and a range of stiffnesses close to that of the fish, and oscillated the models back and forth near the head. The tail amplitude decreased monotonically as frequency increased from 2 Hz to 4 Hz, regardless of stiffness (McHenry et al., 1995).

Although the impact of resonance was not clear in that study, further studies by Long and colleagues demonstrated that body stiffness and damping clearly have an effect on swimming (Long et al., 1996, 2002b; Long and Nipper, 1996; Long, 1998). They hypothesized that fish might stiffen their bodies to swim faster. Long and Nipper (1996) and Long (1998) then developed a device to bend the whole bodies of fish and measure the stiffness, both passively and when the muscles were stimulated to produce force. Indeed, they found that the effective passive stiffness could increase

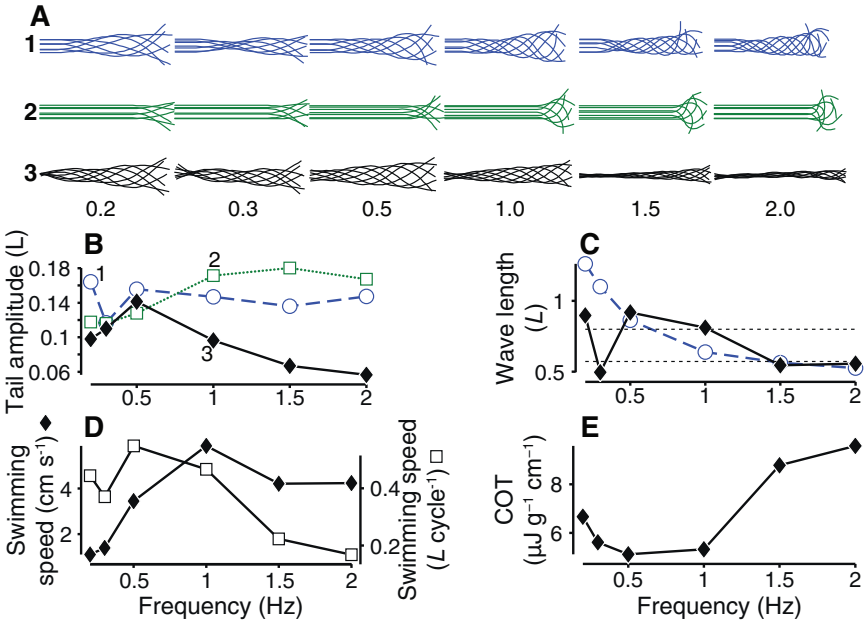

Fig. 2. Complex resonance-like effects in an elongated fish body. Data are computed using the computational fluid dynamic simulation from Tytell et al. (2010). (A) Midline traces for one bending cycle at a range of frequencies for: (case 1) passive bending when the head region (first 30%) oscillates up and down over 1 cm and most of the body is free to move; (case 2) passive bending when most of the body oscillates over 1 cm and only the last 30% is free to bend; (case 3) free swimming with a traveling muscular activation wave at a range of frequencies. (B) Amplitude of the resulting tail motion. (C) Normalized body wavelength for the first passive trial (case 1) and active swimming (case 3). Wavelengths were too short to be estimated in case 2. The dashed lines show the wavelengths of the second and third Euler-Bernoulli bending modes. (D) Absolute and nondimensional swimming speed for the active swimming case (case 3; left axis: absolute speed, filled diamonds; right axis: nondimensional speed, open squares). (E) Cost of transport for the active swimming trials (case 3).

substantially if the muscles were activated at a particular phase in the bending cycle, for largemouth bass (*Micropterus salmoides*) (Long and Nipper, 1996) and American eels (*Anguilla rostrata*) (Long, 1998). Tests on living fish were more difficult to interpret: as expected, cutting the collagenous fibers in the dermis of longnose gar (*Lepisosteous osseus*) reduced the stiffness of the body (Long et al., 1996). If the gar's body is like an elastic beam (Long et al., 2002a), this reduced stiffness would also reduce the resonant frequency, and tail beat frequency did decrease when the skin was cut, perhaps suggesting that they were trying to match the resonant frequency (Long et al., 1996). However, the fish compensated for the lower frequencies by spreading their tails, which allowed them to swim faster for the same tail beat frequency after the surgical reduction in body stiffness (Long et al., 1996). Along with the skin, the notochord of hagfishes (*Myxine glutinosa*) may contribute to the stiffness and damping properties of the whole body (Long et al., 2002b). More recently, however, Nowroozi and Brainerd (2013) examined the escape responses of a striped bass (*Morone saxatilis*) using high-speed X-ray videography, and concluded that, even in this extreme behavior, the intervertebral joints were not sufficiently strained to contribute to the whole body stiffness.

These studies showed the importance of body stiffness, but not necessarily resonance. Other tests have demonstrated resonance. Leftwich et al. (2012) tested the properties of an elastomer model of a lamprey tail ($E = 0.17$ MPa), and they did find a resonant peak. They oscillated the model from side to side in water and found a distinct resonant peak at 0.28 Hz. When they attached the tail to a lamprey robot that swam at the resonant frequency, they found that the robot produced substantially more thrust than when the same tail was oscillated at a higher frequency (Leftwich et al., 2012). Similarly, Kemp et al. (2003) tested a rubber fin for use as a propulsor on an underwater vehicle. They found a peak in the thrust force relative to the input power at 6 Hz and a 90° phase offset between torque and angular velocity, an indication of resonance (e.g., Fig. 1B). Spagnolie et al. (2010) examined a rigid plate attached to a torsional spring, using both experiments and computations. When they flapped the plate up and down, it would pitch passively and propel itself forward. The fastest forward velocity occurred at a frequency close to, but slightly larger than, the resonant frequency, both for their experimental model that was much denser than water, and for a computational model that was very close to the density of water (Spagnolie et al., 2010).

Animals other than fish may also benefit from resonant effects. The hydromedusan jellyfish *Polyorchis penicillatus* may swim close to the resonant frequency of its bell (DeMont and Gosline, 1988). Cheng et al. (1996) suggested that a swimming scallop (*Placopecten magellanicus*) may also benefit from the resonance of the hinge joint, although they also found that the average jetting frequency (around 3 Hz) was substantially lower than their estimated resonant frequency (about 4.5 Hz).

The simple concept of a one-degree-of-freedom resonance (like in Eq. (3)) becomes much more complicated in an elongated body like a fish's. Small-amplitude oscillations of fairly stiff, slender beams have been studied in detail (see textbooks such as Hartog, 1985). Beams have oscillation modes that (roughly) correspond to the number of bends along the beam, each mode with its own resonant frequency, and, provided the oscillations are small, the actual motion can be represented as a sum of the different bending modes. For instance, according to Euler–Bernoulli beam theory, a slender vibrating beam with both ends free has resonant frequencies (Han et al., 1999)

$$f_i = \sqrt{\frac{EI}{\rho_b S L^4}}\frac{2\pi}{\lambda_i^2}, \quad i \in 1, 2, \ldots, \infty, \tag{5}$$

where EI is the bending stiffness of the beam, ρ_b is its density, S is its cross-sectional area, L is its length, and λ_i are the normalized wavelengths of the bending modes. Higher modes have shorter wavelengths; if the ends are free, $\lambda_i \approx 2/(i + 0.5)$. Thus, higher modes have higher resonant frequencies.

However, Euler–Bernoulli beam theory is only appropriate for small-amplitude oscillations ($A < 0.05\,L$) (Hartog, 1985), which is

not true for most fishes (Videler, 1993). Also, many fishes are not slender, as defined in this theory: Euler–Bernoulli beam theory is best for diameters less than 0.04 L (Han et al., 1999). If amplitudes are large or beams are not slender, higher modes do not necessarily have higher resonant frequencies, and the mode shapes have complicated relationships with the shape and slenderness of the beam (Han et al., 1999). Moreover, fluid dynamic effects, including vortex shedding and viscous drag, can damp out or alter resonant effects (Fig. 1; Aureli and Porfiri, 2010).

For example, Fig. 2 shows some of the complexity of oscillatory bending of an elongate body in a fluid. Using a two-dimensional computational fluid dynamic simulation of a lamprey body (Tytell et al., 2010), the head region (first 30%) was forced to oscillate, allowing most of the body to flex passively in the fluid (blue traces and symbols in Fig. 2A). Alternatively, to minimize the effects of different bending modes, the first 70% of the body was forced to oscillate, allowing flexing only in the last 30% (green traces and symbols in Fig. 2A). These two tests were compared to the free-swimming performance, in which the body is actuated by a traveling wave of muscle activity with a wavelength of 1 L (black symbols in Fig. 2A); the resulting mechanical wave does not necessarily have the same wavelength (Tytell et al., 2010). The bending stiffness of lamprey bodies is not known; the computational model has a Young's modulus of 0.76 MPa, which is close to that of eels and hagfishes (Long, 1998; Long et al., 2002b). See Section 6.1 below for further details.

Bending tests showed several potential resonant frequencies, depending on the bending mode. For body oscillations, bending at frequencies below 1 Hz exhibited complex effects, with a possible resonant peak at 0.5 Hz (Fig. 2B, open blue circles). Some of this complexity may be related to the fact that different bending modes are excited at different frequencies; body wavelength (which corresponds to bending modes) for passive bending changes rapidly at low frequencies (Fig. 2C, blue symbols). In contrast, tail oscillations excited a higher bending mode, as expected, with a resonant frequency near 1.5 Hz (Fig. 2B, open green squares).

These resonant peaks seem to depend on fluid forces. The Euler–Bernoulli beam frequencies (from Eq. (5)) for this body model, with no fluid forces, are much higher than we observed in the simulations. For example, the first resonant frequency is 3.2 Hz, corresponding to a wavelength of 3.3 L. The next higher modes have wavelengths of 1.34 L and 0.80 L, which are closer to the wavelengths observed (Fig. 2C, dashed lines) but have much higher resonant frequencies.

Free swimming showed another set of effects. Keeping all parameters constant aside from actuation frequency, the largest tail amplitude occurs at 0.5 Hz (Fig. 2B, filled diamonds), which corresponds to the fastest normalized swimming speed in lengths traveled per tail beat cycle (Fig. 2E, filled diamonds). This frequency does not produce the highest absolute swimming speed (in cm/s), however; that occurs at 1 Hz. A broad minimum in cost of transport (Schmidt-Nielsen, 1997) of about 5 $\mu J\,g^{-1}\,cm^{-1}$ occurs between 0.5 and 1 Hz, and is close to the measured cost of transport of 4.2 $\mu J\,g^{-1}\,cm^{-1}$ for eels swimming at 0.5 $L\,s^{-1}$ (van Ginneken et al., 2005). Thus, a tail beat frequency of 0.5 Hz uses the least energy to cross a distance, but it takes only marginally more energy to swim at 1 Hz and cross the same distance almost twice as quickly.

4. Can fish sense mechanical resonance?

Based on these mechanical arguments and data, it is not clear how important resonance is for swimming fish. If resonance is important, however, it would make sense that fish would evolve ways to sense it. Resonance has two key features that fish may be able to sense. The first is the peak in gain near the resonant frequency (Fig. 1A). Though this peak seems important, the shift in phase around the resonant frequency (Fig. 1B) may be more relevant for locomotor control.

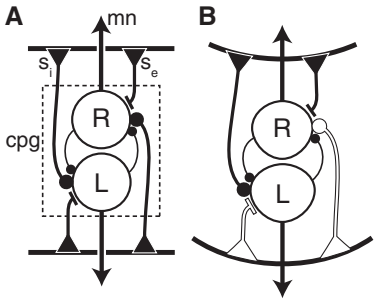

Fig. 3. Schematic of the connections between a generic central pattern generator (CPG) and proprioceptors, based on the lamprey. (A) Lines ending with circles or bars represent inhibitory or excitatory connections, respectively. The CPG is shown as two mutually inhibitory half centers (labeled R and L). There are two classes of proprioceptors: a crossed inhibitory class, labeled s_i, and an ipsilateral excitatory class, s_e. Right and left motor neurons (mn) are shown with arrows. (B) Example of the effect of a bend toward the right. The left proprioceptors are excited by the curvature, and are shown with open symbols.

Consider the schematic of a locomotor CPG circuit in Fig. 3A (after Viana Di Prisco et al., 1990). As is typical, the CPG consists of two mutually inhibitory "half-centers" (labeled 'L' and 'R'; Fig. 3A). The proprioceptive sensory cells (triangles), modeled after the lamprey's edge cells, respond to body bending by sensing stretch in the margins of the spinal cord (upper and lower thick lines). One population excites the ipsilateral half-center; the other inhibits the contralateral side (Viana Di Prisco et al., 1990). Flexor and extensor muscle spindles in tetrapods have similar crossed inhibitory connections (Rossignol et al., 2006). Rhythmic stimulation of the proprioceptors over a range of frequencies can entrain the CPG's rhythm, forcing it to match the stimulus frequency (McClellan and Sigvardt, 1988; Rossignol et al., 2006; Tytell and Cohen, 2008).

Although proprioceptors like edge cells or muscle spindles have not been conclusively identified in teleost fishes, comparative studies of cells in the vertebrate spinal cord suggest that they may have mechanoreceptors like edge cells. Cells called marginal nuclei that resemble mechanoreceptors and have a morphology and location in the spinal cord similar to those of edge cells are present in snakes (Schroeder, 1986), salamanders (Chevallier et al., 2008; Schroeder and Egar, 1990), birds (Rosenberg and Necker, 2000) and elasmobranchs (Anadón et al., 1995). If marginal nuclei are mechanoreceptive like edge cells, as their morphology indicates, then their wide distribution among vertebrates suggests that teleost fishes should also possess edge-cell-like proprioceptors.

The phase relationship that is typical of resonance, together with the wiring of proprioceptors, may allow a CPG circuit to match a resonant frequency. Specifically, crossed inhibitory proprioceptors may push the frequency higher when the system is below its resonant frequency, and push the frequency lower when the system is above its resonant frequency. At frequencies below the resonant frequency, force is in phase with local curvature. In Fig. 3B, below the resonant frequency, muscle on the right side would therefore be producing force to cause the curvature shown. The left-side proprioceptors are stretched, inhibiting right-side activity and exciting left-side activity, resulting in a shorter motor burst and a more rapid transition from activity on one side to activity on the other. The net effect, then, is to increase the cycle frequency. At frequencies above the resonant frequency, the opposite would be true. At high frequencies, the force is 180° out of phase with the local curvature, meaning that the left-side muscle would be active during the curvature shown in Fig. 3B. The left proprioceptors are also stretched, exciting left-side activity and inhibiting the right side, extending

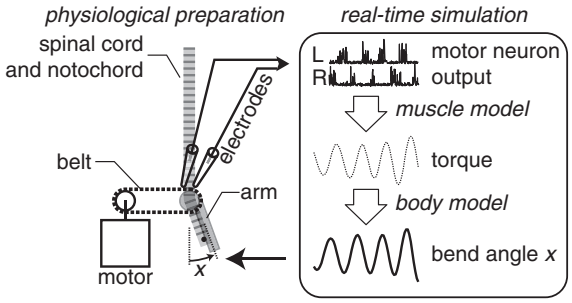

Fig. 4. Diagram of the closed-loop preparation. Motor output from a physiological preparation of the lamprey spinal cord is sampled and used in a real-time simulation of the muscle and body, which computes a bend angle *x*. The bend angle is fed back to the preparation using a motor that bends the spinal cord and notochord.

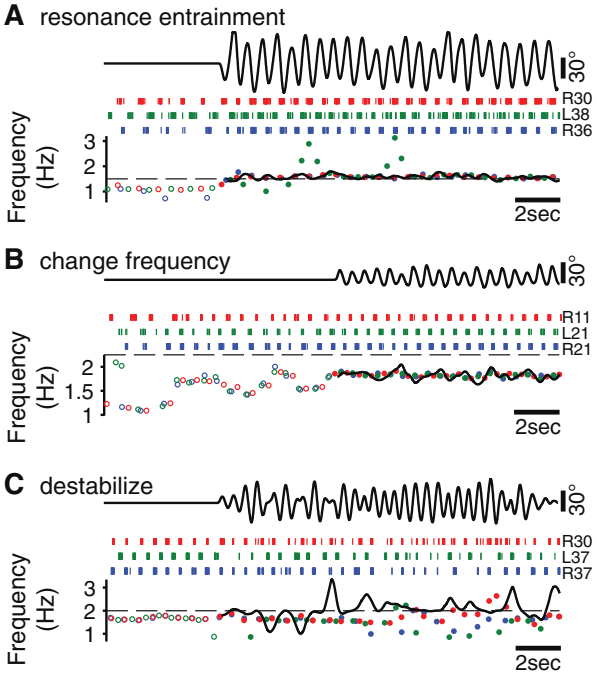

Fig. 5. Examples of different effects from closed-loop stimulation. In each panel, the top black trace shows the bend angle, the middle raster plot shows the spike times from three motor nerve recordings, labeled according to segment number, and the bottom plot shows the frequency of the bursts (circles) and the bending (black line). The blue and green channels are recorded close to the point of bending, while the red channel is further away. The dashed line shows the resonant frequency. Filled symbols indicate when the stimulus is on. (A) Resonance entrainment. Burst frequency (circles) and stimulus frequency (thick line) match the resonant frequency (dashed line). (B) Change in frequency and stabilization of the burst rhythm, but burst and stimulus frequency are below the resonant frequency. Variability in frequency is reduced after the stimulus is turned on (compare open and closed circles). (C) Destabilization of a stable rhythm. Six seconds after the beginning of the trial, the bursts become quite irregular and do not match either the stimulus frequency (solid line) or the resonant frequency (dashed line).

the motor burst and delaying the transition from one side to the other. These effects may also interact with the intrinsic oscillation frequency of the CPG.

Computer and physical models support the idea of resonance entrainment in simple CPG topologies like that of Fig. 3. Several groups (Iwasaki and Zheng, 2006; Williams and DeWeerth, 2007; Futakata and Iwasaki, 2008) have examined mathematical models of a reciprocally inhibitory oscillator (as in Fig. 3), coupled to a pendulum with various feedback mechanisms. They termed the proprioceptive connections in Fig. 3 "negative" feedback; a reversed diagram, with crossed excitatory connections or ipsilateral inhibitory connections, would be "positive" feedback. In general, they found that, for sufficiently high feedback gain (the strength of the proprioceptive synapses) and for a lightly damped mechanical system, negative proprioceptive feedback can produce robust resonance entrainment, particularly when the CPG baseline frequency is smaller than the mechanical resonant frequency. Physical models also show similar resonance entrainment (Williamson, 1998; Verdaasdonk et al., 2006; Pelc et al., 2008).

However, it is not clear whether these results extend to locomotor control in fish. As discussed above, the resonance is probably highly damped. Also, fish bodies are elongated, and sensory input is distributed along the body. Thus, the simple wiring diagram presented in Fig. 3 may be incomplete, or possibly incorrect (Parker, 2006). Edge cells, the proprioceptor in lampreys, for example, have axons that extend at least 20% of the body away from the point of local curvature, primarily in the rostral direction (McClellan and Sigvardt, 1988; Rovainen, 1982). Moreover, the impact of edge cells on the CPG seems to differ along the body, with rostral edge cells entraining the CPG at a phase almost 180° different from the effect of caudal edge cells (Tytell and Cohen, 2008; Hsu et al., 2013).

To examine resonance entrainment in the lamprey, we developed a closed-loop preparation (Fig. 4). We recorded activity in the ventral root motor nerves of a fictively swimming preparation of the lamprey. In a real-time computer simulation, we estimated the muscular force that would develop from the ongoing motor activity, and used that force as an input to a simulated harmonic oscillator (Eq. (2)). We compared the effects of two different types of muscle models: a simple low-pass linear filter with a variable lag, and a Hill-type muscle model with calcium dynamics (Williams et al., 1998; McMillen et al., 2008). The real-time simulation then computed the bending angle that would result from the ventral root activity and fed that back as a bending stimulus to the spinal cord. Using this preparation, we could test the same spinal cord preparation from one animal with many different simulated mechanical parameters. We focused on the resonant frequency, the muscle model, the gain, and the damping ratio to examine resonance entrainment. Other groups are developing similar approaches (Richards, 2011; Edwards et al., 2013; Richards and Clemente, 2013). See Section 6 for further details.

For simplicity, we simulated only one "joint" using a single-degree-of-freedom harmonic oscillator with no fluid forces. The model is therefore useful to determine whether the CPG can tune in to a mechanical resonance at a single point, but it does not address the complex resonance properties of elongated bodies or the effects of fluid forces.

We tested five individuals with the closed-loop protocol. Parameters examined included the resonant frequency (range from 1 to 2.5 Hz), damping ratio ζ (at values 0.01, 0.1, 0.5, 1), and gain. Gain was scaled so that a gain of ± 1 produced an amplitude of approximately 30°; within that range, we tested gain values from -1 to 1 in steps of 0.05, except for a gain of 0. We also compared parameters within the two muscle models. For the linear filter, parameters included the filter cutoff (2, 3, and 4 Hz) and lag (50, 100, 200, 300, and 500 ms). For lamprey muscle, the typical time from an action potential to peak twitch force is approximately 200 ms (Buchanan and Cohen, 1982), within the range of filter parameters that we used. In the muscle model, we tested the effects of the force – length and force – velocity relationships by setting force not to vary with length and/or velocity, or to vary in a physiologically accurate way (Williams et al., 1998).

Effects were highly variable. Resonance entrainment was observed (Fig. 5A). We also observed that closed-loop stimulation could change and stabilize the system frequency, without entraining to the resonant frequency (Fig. 5B). Closed-loop stimulation also often destabilized the system (Fig. 5C).

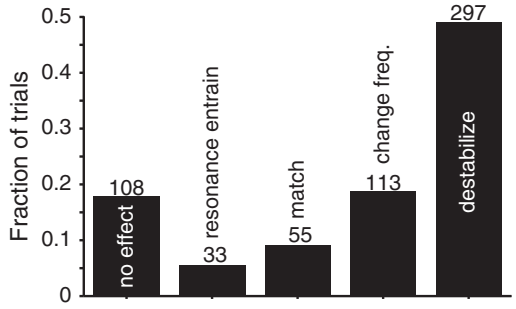

Fig. 6. Summary of the number of trials with different effects. Clear resonance entrainment is separated from "match", when the system oscillated at the resonant frequency, but the resonant frequency was not sufficiently different from the baseline. "Change freq." represents the trials when the system changed frequencies, but not to match the resonant frequency. "Destabilize" means that the rhythm was not stable.

Fig. 6 shows a summary of the number of trials that produced different effects. Many trials (18%) resulted in no substantial change in the system frequency or variability. The most common effect (48% of trials) was to destabilize the system, increasing the cycle variability (see Section 6.2 for definition). Many other trials (17%) changed frequency, but not to match the resonant frequency. True resonance entrainment (8% of trials) could only be identified when the system frequency changed sufficiently from its baseline; in other cases (9%), the system frequency matched the resonant frequency, but system frequency was not far enough away from the baseline to unequivocally identify resonance entrainment.

Although most trials did not produce resonance entrainment, there were some commonalities among those that did (Fig. 7). Significant effects of the model parameters were tested by tabulating the number of trials with different effects and testing for deviations from uniformity using maximum likelihood (Quinn and Keough, 2002).

Modeling results (Iwasaki and Zheng, 2006; Williams and DeWeerth, 2007) suggested that high gain, whether positive or negative, should produce resonance entrainment in some range of resonant frequencies. We found that gain had a significant effect ($G^2 = 24$; $P = 0.001$). Low positive gains tended not to produce resonance entrainment, but if they did, they entrained below the baseline. Negative gains and larger positive gains were more likely to entrain above the baseline (Fig. 7B).

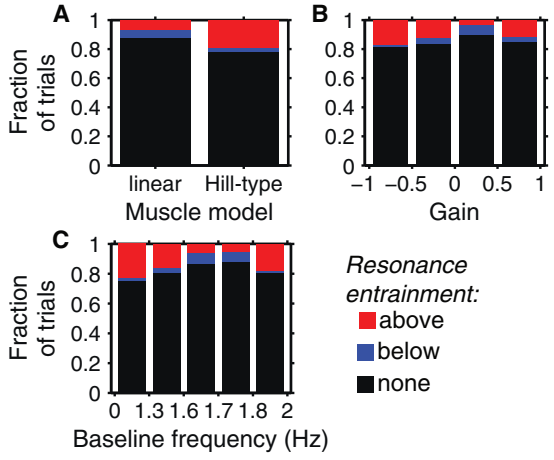

Fig. 7. Effects of different simulation parameters on resonance entrainment. In all cases, the largest fraction of trials did not produce resonance entrainment (black bars). The fractions of trials that produced resonance entrainment above or below the baseline frequency are shown in red and blue, respectively. (A) Effect of the muscle model, either a linear filter or a Hill-type model. (B) Effect of gain. Each bar represents a bin of several different gain values. (C) Effect of the intrinsic baseline frequency. Bars represent frequency bins.

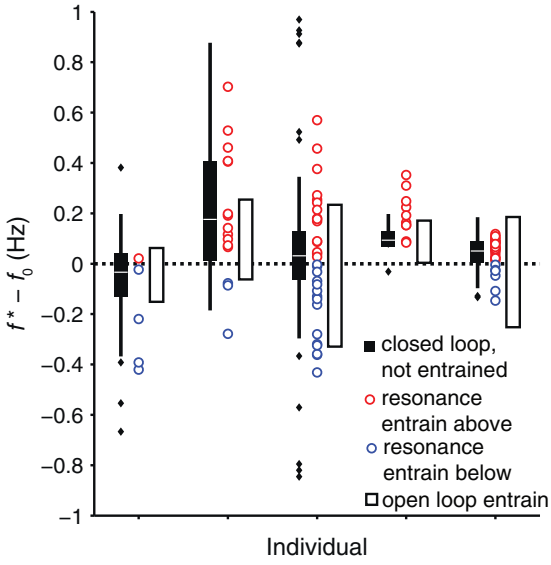

Fig. 8. Differences in open- and closed-loop entrainment ranges among individuals. For each individual, a filled box plot shows the range of closed-loop frequencies that were not entrained to the resonant frequency, where the box ranges from the 25 to 75 percentile and the white line is at the median. Outliers, shown as diamonds, are outside 1.5 the inter-quartile range. Red and blue points indicate trials with resonance entrainment above or below the baseline, respectively. Open boxes indicate the open-loop entrainment range.

Damping did not have a significant effect ($G^2 = 14$; $P = 0.08$), although the trend suggested that underdamped systems might entrain below the baseline more often than critically damped or overdamped systems. None of the parameters of the muscle models had significant effects, but the type of model was important ($G^2 = 15$; $P = 0.001$; Fig. 7A). When entrainment occurred, the linear filter was far more likely to entrain below the baseline frequency, while the Hill-type model entrained almost exclusively above the baseline (Fig. 7A).

We also observed that the properties of the preparations themselves were important in resonance entrainment (Fig. 7C). The intrinsic baseline frequency had a significant effect ($G^2 = 24$; $P = 0.001$). Preparations with a relatively slow burst frequency were more likely to entrain in general, and particularly above the baseline frequency, whereas those with high frequencies tended not to entrain or to entrain below the baseline (Fig. 7C).

Although the effects differed substantially across individuals, closed-loop stimulation could almost always entrain the CPG system above the open loop entrainment range. Fig. 8 shows the differences among individuals for the system frequency f^* relative to the baseline frequency f_0 during closed-loop stimulation without resonance entrainment, during resonance entrainment above and below the baseline, and during open-loop entrainment. In all but one individual, closed-loop stimulation could entrain the system outside of the open loop range.

5. Whither resonance?

The data and arguments presented here represent, to some extent, a negative result. We argue, first, that movement may be highly damped in water, and second, that resonance may be very complex and perhaps not all that hydrodynamically relevant for elongated swimming fishes that swim with an anguilliform mode. Then we show data that suggest that CPGs, as modeled by that of the lamprey, may not as easily entrain to a resonant frequency as computational models have suggested (Hatsopoulos,

1996; Williamson, 1998; Iwasaki and Zheng, 2006; Williams and DeWeerth, 2007).

In a fish with an elongated body and a distributed CPG, resonance and resonance entrainment may simply be a more complex phenomenon than in the single-degree-of-freedom systems that have been analyzed in the past. In particular, it may be that a fish's CPG is tuned to amplify a particular bending mode. Our single-point bending apparatus would not be able to detect such an effect.

Indeed, our apparatus may be more appropriate for other fishes. Lampreys, like eels, swim in the anguilliform mode, in which most of the body undulates. Many other fishes swim differently, using modes called carangiform and thunniform, in which oscillation primarily occurs in the tail region (Lauder and Tytell, 2006) and bending is closer to the single-point bending used here. This type of bending seems to produce a simpler resonant effect at a more appropriate frequency (Fig. 2; green symbols), which might be more relevant to swimming. Carangiform and thunniform swimmers, particularly tunas and other scombrid fishes, have much stiffer bodies than elongate anguilliform swimmers (Aleyev, 1977), and so they may be less affected by fluid dynamic damping.

Similar closed-loop tests could be useful for understanding other complex neuromechanical systems (Richards, 2011; Edwards et al., 2013; Richards and Clemente, 2013). Our experience suggests several important methodological considerations. First, unsurprisingly, optimization of the loop rate and jitter of the real-time system is crucial. Initial versions of the system used Matlab or LabView running under Windows and could not run the simulation faster than 20 Hz, which introduced artificial instabilities. Even at 20 Hz, occasional large delays introduced by the multitasking operating system caused problems. The current version runs at 100 Hz using a dedicated real-time operating system (LabView Real-Time module 2009; National Instruments, Austin, TX, USA). Second, we took care to ensure that recordings from each side of the body were well matched, with similar numbers of units and amplitudes, so that they could be used as inputs to the muscle model. Each channel was also scaled independently so that they had a peak amplitude of unity. This requires gain to be relatively low. Amplitude of the bending signal corresponds approximately to the strength of the response in the edge cells (Grillner et al., 1984), but amplitude cannot increase above about $\pm 30^{\circ}$ without risking mechanical damage to the preparation. Since amplitude increases with increasing gain, the gain in the simulation must remain relatively low.

Interestingly, the class of muscle model seems to be important; a more physiological model produces more resonance entrainment (Fig. 7A). A Hill-type muscle model can be solved very efficiently in real time, and though it adds more parameters to the model, does not represent an increase in numerical complexity. Further work will investigate the effects of the muscle nonlinearities in more detail.

Clearly, resonance in elongated fish bodies is complex. Moreover, it may not directly correlate with the fastest swimming speed, or the most efficient (Fig. 2). A further consideration is that a resonant frequency may not necessarily align best with the hydrodynamic demands of swimming. For effective swimming, vortices must be shed appropriately into the wake (Hover et al., 2004; Buchholz and Smits, 2006; Green and Smits, 2008). Undulating at a resonant frequency may not necessarily shed vortices at the right times to develop a good wake structure for swimming, and thus it may not result in efficient propulsion even if it reduces the energy demands for oscillation. Ramananarivo et al. (2011) found this effect when they studied flexible flapping propulsors. They found that flapping below the resonant frequency resulted in optimal cambering of the wing, so that vortices are shed smoothly into the wake. At the resonant frequency, flow tended to separate around the wing, resulting in lower thrust.

Additionally, resonance is not the only mechanical instability that may contribute to propulsion. One intriguing possibility is that elongate fishes may be able to harness the same instability that leads to flapping in flags (Shelley and Zhang, 2011). This effect is different from resonance because it is a result of the coupling between the body and the fluid, rather than a property of the body alone, and can occur for bodies with very low stiffness. Perhaps fishes like lampreys are closer to flapping flags, while tunas are more similar to bouncing springs. Understanding these passive mechanical effects will be crucial to understanding the speed and efficiency of swimming in aquatic organisms.

6. Methods

6.1. Computational fluid dynamic methods

The coupled fluid–elastic system of the swimmer described above (Section 3) was simulated using an immersed boundary framework (Peskin, 2002) with the same body model as presented in Tytell et al. (2010). The full, incompressible two-dimensional (2D) Navier–Stokes equations are solved on a multi-level Cartesian grid. The elastic body of the swimmer is accounted for by a Dirac delta-function layer of force in the Navier–Stokes equations, supported by the region of fluid that coincides with the material points of the body. At each time step, the no-slip condition at the immersed boundary is enforced by moving its material points at the updated and interpolated fluid velocity. Adaptive mesh refinement that tags spatial grid cells containing the immersed boundary or those with large vorticity allows the capturing of boundary layers and vortex shedding at high Reynolds numbers (Griffith et al., 2007).

The solution of the Navier–Stokes equations is formally second-order accurate in both time and space (Griffith et al., 2007). Because adaptive mesh refinement is used, fluid flow in the narrow boundary layer around the lamprey and in the vortex wake is well resolved. We have performed detailed convergence studies where both the levels of grid refinement and the tagging thresholds of the vorticity are varied, and we note that convergence has been reached. The simulations discussed in this manuscript have been implemented using numerical parameters that are well within this convergent range.

The computational swimmer, whose length is $L = 12.6$ cm, is built out of three segmented filaments: a stiff center line ("backbone") with 640 links, and two lateral sides with 320 links. The structure reproduces, abstractly, the geometry and mechanical properties of fish bodies. Links along the backbone and crosslinks to the two sides are Hookean springs; links along the sides are also springs, but they only resist extension, not compression (similar to collagen fibers). The side links can also actively produce force, using a Hill-type muscle model after McMillen et al. (2008).

Cost of transport is estimated by computing the total positive muscle work $W_+ = \int_{T_i}^{T_{i+1}} -F_{mus}(\partial l/\partial t)dt, (\partial l/\partial t) < 0$, where F_{mus} is the force produced by the muscle segment and l is the length of the segment, and the total negative muscle work $W_- = \int_{T_i}^{T_{i+1}} -F_{mus}(\partial l/\partial t)dt, (\partial l/\partial t) > 0$. Metabolically, negative work requires approximately 0.2–0.25 times the energy in comparison to positive work (Ruina et al., 2005), and thus cost of transport is estimated as $COT = \Sigma(W_+ - 0.25W_-)f/mU$, where f is the tail beat frequency, and U is the steady swimming speed. The mass m of the 2D swimmer is estimated as the mass of a tapered cylinder with a constant height, equal to the mean width of the swimmer, and the same density as water.

6.2. Closed-loop preparation

Preparations from five individual lampreys were tested. All animal procedures were conducted at the University of Maryland, College Park, and were approved by the UMCP Institutional Animal Care and Use Committee.

First, fictive swimming was induced in a preparation of the spinal cord and notochord, following Tytell and Cohen (2008). A lamprey is lightly anesthetized using a buffered solution of 0.2 g/l tricaine methanesulfonate (MS222; Sigma), then rapidly decapitated and eviscerated. Skin and muscle are carefully peeled away from the notochord, taking care to avoid damaging the motor nerves that run along the notochord. All membranes dorsal to the spinal cord are carefully removed. Between 50 and 60 segments between the last gill slit and the anus are exposed. For consistency, preparations were cut so that they contained 30 segments. The spinal cord and notochord preparation is then transferred to a bath of physiological saline (NaCl: 91 mM, KCl: 2.1 mM, $CaCl_2$–$2H_2O$: 2.6 mM, $MgCl_2$–$6H_2O$: 1.8 mM, glucose: 4.0 mM, $NaHCO_3$: 20.0 mM) at 9 °C. The notochord is attached to a computer-controlled motorized arm.

Two components of the feedback loop are simulated in real time (Fig. 4). To record the input signal, electrodes are placed on motor nerves on the left and right sides of the same segment or adjacent segments, close to the point of bending. We also recorded a third channel further away from the bending point. The signal is rectified and scaled so that signals from both sides have amplitude 1. The signal is used as an input for two different classes of muscle models. The first is a simple finite impulse response linear low-pass filter with an adjustable cutoff frequency and lag. Filters were designed using a complex Chebyshev approximation that allows filter order, cutoff frequency, and lag to be independently specified (Karam and McClellan, 1995; implemented in Matlab's cfirpm routine). The second model is a Hill-type muscle model, which uses the neural activity as an activation signal (after McMillen et al., 2008). This model produces an estimate of the muscle force from each side of the body; the difference of the left and right sides is multiplied by a gain value and used as the forcing F_{in}/m due to muscle (Eq. (2)). Gain is scaled for each preparation by examining the estimated output without actually applying the bend to the preparation. We scaled gain so that a gain of 1 produces a displacement of about 30° without feedback. We then solve Eq. (2) for x, which in this case is a bending angle, and the body is bent through that angle by the motorized arm (Fig. 4).

The real-time simulation is implemented in the LabView Real-Time module with a dedicated computer running the National Instruments Real-Time operating system and sampling data with a PCI-6221 data acquisition card. The simulation runs at a 100 Hz loop rate, which is near the maximum spike rate and therefore sufficiently fast to account for the feedback loop. Between 100 and 220 trials of different simulated mechanical parameters were tested on a single spinal cord preparation. Each trial lasted at least 30 s, and most combinations of parameters were tested twice. Experiments lasted for 6–8 h; previous results have shown consistent results in the lamprey preparation over this time period (Tytell and Cohen, 2008), and no degradation of the preparation was observed.

Resonance entrainment was defined as when the system frequency f^* was within 5% of the resonant frequency f_{res}.

To quantify variability, we computed the autocorrelation $R(\tau)$ of the spike rates for each channel, where τ is a time lag. For a periodic signal, $R(\tau)$ will have peaks at $\tau = nT$, $n = 1, 2, \ldots$, where T is the cycle period. The height of the first autocorrelation peak indicates how well each burst is correlated with the next; we use $v = 1 - R(\tau = T)$ as a measure of the variability.

We also measured the open-loop entrainment range (as in Tytell and Cohen, 2008) using a 30° amplitude sinusoidal stimulus that gradually increased in frequency. Entrainment was present when there was one CPG burst per stimulus cycle.

6.3. Statistics

We used contingency tables (Quinn and Keough, 2002) to test whether resonance entrainment was significantly affected by different parameters in the closed-loop preparation. First, the baseline burst frequency with no stimulus was estimated in the 10 s preceding each trial. Trials were then grouped into those that did not produce resonance entrainment, those that entrained above the baseline frequency, and those that entrained below the baseline. Most parameters had several discrete values, resulting in a $n \times 3$ table, where n is the number of values for the parameter. To examine the effect of gain, the baseline frequency, and the baseline variability, we binned the values. If the parameter has no effect on resonance entrainment, the frequencies should be independent across the table (Quinn and Keough, 2002). Significance was assessed using the G^2 likelihood ratio statistic, which follows a χ^2 distribution (Quinn and Keough, 2002).

Acknowledgments

Funding for this research was provided by the National Institutes of Health (CRCNS R01 NS054271, to Avis H. Cohen), by the National Science Foundation (RCN-PLS DBI 1062052, to L.J.F.), and by the Army Research Office (W911NF1110495, to E.D.T.; Samuel Stanton, program officer). Jessica Barber of the U.S. Fish and Wildlife Service provided the lampreys. The authors gratefully acknowledge the help and support of Avis Cohen. Two anonymous reviewers helped to improve the manuscript substantially.

References

Ahlborn, B.K., Blake, R.W., Megill, W.M., 2006. Frequency tuning in animal locomotion. Zoology 109, 43–53.
Aleyev, Y.G., 1977. Nekton. Junk, The Hague, Netherlands.
Anadón, R., Molist, P., Pombal, M.A., Rodríguez-Moldes, I., Rodicio, M.C., 1995. Marginal cells in the spinal cord of four elasmobranchs (*Torpedo marmorata*, *T. torpedo*, *Raja undulata* and *Scyliorhinus canicula*): evidence for homology with lamprey intraspinal stretch receptor neurons. Eur. J. Neurosci. 7, 934–943.
Aureli, M., Porfiri, M., 2010. Low frequency and large amplitude oscillations of cantilevers in viscous fluids. Appl. Phys. Lett. 96, 164102.
Buchanan, J.T., Cohen, A.H., 1982. Activities of identified interneurons, motoneurons, and muscle fibers during fictive swimming in the lamprey and effects of reticulospinal and dorsal cell stimulation. J. Neurophysiol. 47, 948–960.
Buchholz, J.H.J., Smits, A.J., 2006. On the evolution of the wake structure produced by a low aspect ratio pitching panel. J. Fluid Mech. 546, 433–443.
Cheng, J., Davison, I., Demont, M., 1996. Dynamics and energetics of scallop locomotion. J. Exp. Biol. 199, 1931–1946.
Chevallier, S., Jan Ijspeert, A., Ryczko, D., Nagy, F., Cabelguen, J.-M., 2008. Organisation of the spinal central pattern generators for locomotion in the salamander: biology and modelling. Brain Res. Rev. 57, 147–161.
DeMont, M.E., Gosline, J.M., 1988. Mechanics of jet propulsion in the hydromedusan jellyfish, *Polyorchis pexicillatus*. III. A natural resonating bell; the presence and importance of a resonant phenomenon in the locomotor structure. J. Exp. Biol. 134, 347–361.
Edwards, D.H., Chung, B., Bacque-Cazenave, J., Cattaert, D.,2013. Neuromechanical model of reflexes and locomotor rhythms in the crayfish leg. In: Proc. Ann. Comput. Neurosci. Meet. BMC Neurosci. BioMed Central Ltd., Paris, France, p. P55.
Futakata, Y., Iwasaki, T., 2008. Formal analysis of resonance entrainment by central pattern generator. J. Math. Biol. 57, 183–207.
Goodman, L., Riley, M.A., Mitra, S., Turvey, M.T., 2000. Advantages of rhythmic movements at resonance: minimal active degrees of freedom, minimal noise, and maximal predictability. J. Motor Behav. 32, 3–8.
Green, M.A., Smits, A.J., 2008. Effects of three-dimensionality on thrust production by a pitching panel. J. Fluid Mech. 615, 211–220.
Griffith, B.E., Hornung, R.D., McQueen, D.M., Peskin, C.S., 2007. An adaptive, formally second order accurate version of the immersed boundary method. J. Comput. Phys. 223, 10–49.

Grillner, S., 2003. The motor infrastructure: from ion channels to neuronal networks. Nat. Rev. Neurosci. 4, 573–586.
Grillner, S., Williams, T.L., Lagerbäck, P.-Å., 1984. The edge cell, a possible intraspinal mechanoreceptor. Science 223, 500–503.
Han, S.M., Benaroya, H., Wei, T., 1999. Dynamics of transversely vibrating beams using four engineering theories. J. Sound Vib. 225, 935–988.
Hartog Den, J.P., 1985. Mechanical Vibrations. Dover Publications, New York.
Hatsopoulos, N.G., 1996. Coupling the neural and physical dynamics in rhythmic movements. Neural Comput. 8, 567–581.
Hatsopoulos, N.G., Warren, W.H., 1996. Resonance tuning in rhythmic arm movements. J. Motor Behav. 28, 3–14.
Hoerner, S.F., 1965. Fluid-Dynamic Drag. Hoerner Fluid Dynamics, Brick Town, NJ.
Hover, F.S., Haugsdal, O., Triantafyllou, M.S., 2004. Effect of angle of attack profiles in flapping foil propulsion. J. Fluids Struct. 19, 37–47.
Hsu, L.-J., Zelenin, P.V., Grillner, S., Orlovsky, G.N., Deliagina, T.G., 2013. Intraspinal stretch receptor neurons mediate different motor responses along the body in lamprey. J. Comp. Neurol. 521, 3847–3862.
Iwasaki, T., Zheng, M., 2006. Sensory feedback mechanism underlying entrainment of central pattern generator to mechanical resonance. Biol. Cybernet. 94, 245–261.
Karam, L.J., McClellan, J.H., 1995. Complex Chebyshev approximation for FIR filter design. IEEE Trans. Circ. Syst. II 42, 207–216.
Katz, S., Shadwick, R., Rapoport, H., 1999. Muscle strain histories in swimming milkfish in steady and sprinting gaits. J. Exp. Biol. 202, 529–541.
Kemp, M., Hobson, B., Pell, C.A., 2003. Energetics of the oscillating fin thruster. In: Proceedings of the International Symposium on Unmanned Untethered Submersible Technology, Durham, NH, pp. 1–5.
Lauder, G.V., Tytell, E.D., 2006. Hydrodynamics of undulatory propulsion. In: Shadwick, R.E., Lauder, G.V. (Eds.), Fish Biomechanics. Academic Press, San Diego, pp. 425–468.
Leftwich, M.C., Tytell, E.D., Cohen, A.H., Smits, A.J., 2012. Wake structures behind a swimming robotic lamprey with a passively flexible tail. J. Exp. Biol. 215, 416–425.
Long, J.H., 1998. Muscles, elastic energy, and the dynamics of body stiffness in swimming eels. Am. Zool. 38, 771–792.
Long, J.H., Nipper, K.S., 1996. The importance of body stiffness in undulatory propulsion. Am. Zool. 36, 678–694.
Long, J.H., Hale, M.E., McHenry, M.J., Westneat, M.W., 1996. Functions of fish skin: flexural stiffness and steady swimming of longnose gar *Lepisosteus osseus*. J. Exp. Biol. 199, 2139–2151.
Long, J.H., Adcock, B., Root, R.G., 2002a. Force transmission via axial tendons in undulating fish: a dynamic analysis. Comp. Biochem. Physiol. A 133, 911–929.
Long, J.H., Koob-Emunds, M., Sinwell, B., Koob, T.J., 2002b. The notochord of hagfish *Myxine glutinosa*: visco-elastic properties and mechanical functions during steady swimming. J. Exp. Biol. 205, 3819–3831.
McClellan, A.D., Sigvardt, K.A., 1988. Features of entrainment of spinal pattern generators for locomotor activity in the lamprey spinal cord. J. Neurosci. 8, 133–145.
McHenry, M.J., Pell, C.A., Long, J.H., 1995. Mechanical control of swimming speed: stiffness and axial wave form in undulating fish models. J. Exp. Biol. 198, 2293–2305.
McMillen, T., Williams, T.L., Holmes, P.J., 2008. Nonlinear muscles, passive viscoelasticity and body taper conspire to create neuromechanical phase lags in anguilliform swimmers. PLoS Comput. Biol. 4, e1000157.
Mullins, O.J., Hackett, J.T., Buchanan, J.T., Friesen, W.O., 2011. Neuronal control of swimming behavior: comparison of vertebrate and invertebrate model systems. Prog. Neurobiol. 93, 244–269.
Nowroozi, B.N., Brainerd, E.L., 2013. X-ray motion analysis of the vertebral column during the startle response in striped bass, *Morone saxatilis*. J. Exp. Biol. 216, 2833–2842.
Orlovsky, G.N., Deliagina, T.G., Grillner, S., 1999. Neuronal Control of Locomotion: From Mollusc to Man. Oxford University Press, New York, USA.
Parker, D., 2006. Complexities and uncertainties of neuronal network function. Proc. R. Soc. Lond. B 361, 81–99.
Pelc, E.H., Daley, M.A., Ferris, D.P., 2008. Resonant hopping of a robot controlled by an artificial neural oscillator. Bioinsp. Biomimet. 3, 026001.
Peskin, C.S., 2002. The immersed boundary method. Acta Numer. 11, 479–517.
Quinn, G.P., Keough, M.J., 2002. Experimental Design and Data Analysis for Biologists. Cambridge University Press, Cambridge.
Ramananarivo, S., Godoy-Diana, R., Thiria, B., 2011. Rather than resonance, flapping wing flyers may play on aerodynamics to improve performance. Proc. Natl. Acad. Sci. U.S.A. 108, 5964–5969.
Richards, C.T., 2011. Building a robotic link between muscle dynamics and hydrodynamics. J. Exp. Biol. 214, 2381–2389.
Richards, C.T., Clemente, C.J., 2013. Built for rowing: frog muscle is tuned to limb morphology to power swimming. J. Roy. Soc. Interface 10, 20130236.
Rosenberg, J., Necker, R., 2000. Fine structural evidence of mechanoreception in spinal lumbosacral accessory lobes of pigeons. Neurosci. Lett. 285, 13–16.
Rossignol, S., Dubuc, R.J., Gossard, J.-P., 2006. Dynamic sensorimotor interactions in locomotion. Physiol. Rev. 86, 89–154.
Rovainen, C.M., 1982. Neurophysiology. In: Hardisty, M.W., Potter, I.C. (Eds.), The Biology of Lampreys. Academic Press, London, pp. 1–136.
Ruina, A., Bertram, J.E.A., Srinivasan, M., 2005. A collisional model of the energetic cost of support work qualitatively explains leg sequencing in walking and galloping, pseudo-elastic leg behavior in running and the walk-to-run transition. J. Theor. Biol. 237, 170–192.
Schmidt-Nielsen, K., 1997. Animal Physiology, 5th ed. Cambridge University Press, Cambridge.
Schroeder, D.M., 1986. An ultrastructural study of the marginal nucleus, the intrinsic mechanoreceptor of the snake's spinal cord. Somatosens. Motor Res. 4, 127–140.
Schroeder, D.M., Egar, M.W., 1990. Marginal neurons in the urodele spinal cord and the associated denticulate ligaments. J. Comp. Neurol. 301, 93–103.
Shelley, M.J., Zhang, J., 2011. Flapping and bending bodies interacting with fluid flows. Ann. Rev. Fluid Mech. 43, 449–465.
Spagnolie, S.E., Moret, L., Shelley, M.J., Zhang, J., 2010. Surprising behaviors in flapping locomotion with passive pitching. Phys. Fluids 22, 041903.
Tytell, E.D., Cohen, A.H., 2008. Rostral versus caudal differences in mechanical entrainment of the lamprey central pattern generator for locomotion. J. Neurophysiol. 99, 2408–2419.
Tytell, E.D., Hsu, C.-Y., Williams, T.L., Cohen, A.H., Fauci, L.J., 2010. Interactions between internal forces, body stiffness, and fluid environment in a neuromechanical model of lamprey swimming. Proc. Natl. Acad. Sci. U.S.A. 107, 19832–19837.
van Ginneken, V., Antonissen, E., Müller, U.K., Booms, R., Eding, E., Verreth, J., van den Thillart, G., 2005. Eel migration to the Sargasso: remarkably high swimming efficiency and low energy costs. J. Exp. Biol. 208, 1329–1335.
Verdaasdonk, B.W., Koopman, H.F.J.M., van der Helm, F.C.T., 2006. Energy efficient and robust rhythmic limb movement by central pattern generators. Neural Netw. 19, 388–400.
Viana Di Prisco, G., Wallén, P., Grillner, S., 1990. Synaptic effects of intraspinal stretch receptor neurons mediating movement-related feedback during locomotion. Brain Res. 530, 161–166.
Videler, J.J., 1993. Fish Swimming, 1st ed. Chapman & Hall, London.
Williams, C.A., DeWeerth, S.P., 2007. A comparison of resonance tuning with positive versus negative sensory feedback. Biol. Cybernet. 96, 603–614.
Williams, T.L., Bowtell, G., Curtin, N.A., 1998. Predicting force generation by lamprey muscle during applied sinusoidal movement using a simple dynamic model. J. Exp. Biol. 201, 869–875.
Williamson, M.M., 1998. Neural control of rhythmic arm movements. Neural Netw. 11, 1379–1394.